

# Spatial Coherence Loss for Salient and Camouflaged Object Detection and Beyond

Ziyun Yang<sup>1</sup>, Kevin Choy<sup>1</sup>, and Sina Farsiu<sup>1,2,3</sup>

<sup>1</sup>Department of Biomedical Engineering, Duke University, USA

<sup>2</sup>Department of Electrical and Computer Engineering, Duke University, USA

<sup>3</sup>Department of Computer Science, Duke University, USA

## Abstract

Generic object detection is a category-independent task that relies on accurate modeling of objectness. Most relevant CNN-based models of objectness utilize loss functions (e.g., binary cross entropy) that focus on the single-response, i.e., the loss response of a single pixel. Inspired by the human visual system, which first discerns the boundaries of ambiguous regions (i.e., hard regions) before delving into the semantic meaning, we propose a novel loss function, Spatial Coherence Loss (SCLoss), that uses the mutual response between adjacent pixels to suppress or emphasize the single-response of pixels. We demonstrate that the proposed SCLoss can gradually learn the hard regions by detecting and emphasizing their boundaries. Through comprehensive experiments, we demonstrate that replacing popular loss functions with SCLoss can improve the performance of current state-of-the-art (SOTA) salient or camouflaged object detection (SOD or COD) models. We also demonstrate that combining SCLoss with other loss functions can further improve performance and result in the SOTA outcomes for different applications. Finally, as a demonstrative example of the potential uses for other related tasks, we show an application of SCLoss for semantic segmentation. The codes will be released to <https://github.com/TBD> upon acceptance.

## 1. Introduction

Humans can easily segment complex scenes into several parts or objects based on the semantic meaning of each object. Furthermore, they are capable of distinguishing the salient or camouflaged objects from the background based on the inherent *objectness* properties without even knowing what those objects are [1]. In computer vision, objectness represents the likelihood that each pixel is part of a foreground object. Objectness prediction, implicitly or explicitly, is a fundamental component of many computer vision tasks, and a well-trained objectness prediction model can improve downstream tasks such as weakly supervised learning, visual tracking, image retrieval, and

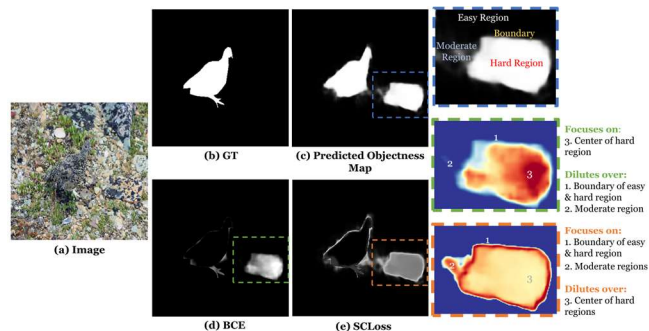


Figure 1. Loss visualization. Given a camouflaged object in (a) and the prediction in (c), the BCE and SCLoss maps are shown in (d) and (e), respectively. The dashed boxes in (c), (d), and (e) contain the same regions that are hard (i.e., the *hard region*), moderately hard (i.e., the *moderate region*), and easy (i.e., the *easy region*) to be distinguished from the foreground. Our SCLoss (e) gives a higher weight to the boundary between the hard and easy regions, and the weights shrink towards the center of the hard region to gradually learn the transition from easy to hard regions, rather than giving high weight to the center of the hard region in (d). Also, SCLoss does not dilute the losses at moderate interference regions.

non-photorealistic rendering [2-5].

Salient and camouflaged object detection (SOD and COD, respectively) are examples of two important tasks wherein modeling objectness plays a crucial role. The goal of SOD is to distinguish the most eye-catching objects from the background, while in COD, that goal is to find the camouflaged objects that are similar to the background [6]. Compared to other relevant tasks such as semantic segmentation [7, 8], where there exist specific classes of interests (e.g., trees, tumors, etc.), SOD and COD proceed in a category-independent manner in which they focus only on the “object” itself rather than its semantic meaning [1].

Among different deep learning models trained on large-scale datasets [9, 10] for SOD and COD tasks, a major category relies on multi-scale learning to leverage the low-level features for obtaining fine-grained details [11, 12] and the high-level semantic features for better scene understanding and object locating [13, 14]. Another category exploits the pixel relationship in the latent space for improving the spatial coherence of the predictions by expanding the receptive fields [15] or using attention mechanisms or vision transformers [16-18].

Most such SOD and COD approaches rely on the single-response category of loss functions, with binary cross

entropy (BCE) being one of the most prominent examples [19]. Single-response loss functions calculate the loss individually for every single pixel without taking the loss responses of surrounding pixels into account. Also, when calculating the overall loss, they weight the loss calculated in each pixel equally, which dilutes the effect of important pixels (e.g., edge pixels) or the foreground pixels when the image is background-dominant. Thus, due to these inherent shortcomings, this loss function group is not necessarily the optimal option for SOD and COD tasks [20-22]. To tackle the latter limitation, some works proposed finding the *hard pixels* (i.e., the foreground/background pixels that are hard to classify correctly; e.g., see Fig. 1) either based on the single-responses [5, 23] or spatial position [21, 24] and giving the harder pixels the larger weights. Unfortunately, this approach unintentionally magnifies the former limitation: since the pixels are still considered individually, wrongly labeled pixels and outlier predictions might be overly weighted, negatively affecting the training stability [23].

To take inter-pixel-responses into account, another class of methodologies [8, 24, 25] converted the objectness prediction task into several inter-pixel connectivity prediction tasks. Of note, to improve the spatial coherence of the predicted objectness maps, i.e., how consistent the predictions are for neighboring pixels that share similar spatial features, [25] proposed to calculate the bilateral probability (mutual response) of two adjacent pixels by multiplying their unilateral probabilities (single response) that describe the likelihood of one pixel belonging to the same class as the other adjacent pixel. However, these methods simply used the acquired mutual response term as the auxiliary output of the network without further exploring its potential to establish loss functions.

Inspired by these methods and the principle of the human visual system, *which usually first discerns the boundaries of ambiguous regions before delving into the semantic meaning* [26, 27], we propose a new scheme for loss function design by using the mutual response between adjacent pixels to suppress or emphasize the single-response of a pixel. Specifically, we propose the spatial coherence loss (SCLoss), in which a mutual response term takes inter-pixel response into account, and a pairwise regularization term further enhances spatial coherence. SCLoss has the following advantages: first, it treats every pixel differently and adaptively adjusts the importance by taking their surrounding pixels’ performance into account; second, it is location-aware and produces a different loss for different pixel pairs (e.g., edge pairs); third, as shown in Fig. 1, compared to BCE in Fig. 1(d) which gives high weights to the entire hard regions and dilutes the moderate regions, the proposed SCLoss in Fig. 1(e) will not dilute the loss response of the moderate regions and most importantly, SCLoss puts more focus on the *boundary between the hard and easy regions* and gradually reduce

the focus as getting to the center of the hard region. These properties enable the network to tackle the hard regions gradually and smoothly by consistently being aware of and learning the transition from easy to hard regions.

Through extensive experiments, we further demonstrate that: 1) the proposed SCLoss can replace the loss functions used in the current state-of-the-art (SOTA) SOD and COD models and improve their performance. 2) The SCLoss is compatible with other well-established loss functions in these two fields [6, 21, 22, 28] and, even when simply treated as an add-on term, can further improve the performance of SOTA models. 3) By instantiating the proposed loss scheme using different single-response loss terms, the proposed SCLoss can potentially improve other downstream tasks, such as semantic segmentation.

## 2. Related Work

### 2.1. Salient Object Detection

CNN-based methods are demonstrated to outperform the early SOD methods, which used handcrafted low-level features and heuristic priors [29-31]. The multi-scale feature aggregation model is a commonly used scheme for deep learning-based SOD. DSS [32] aggregated the multi-scale features using short connections between layers. GCPA [33] learned the global context information at different stages of layers to establish the relationship between salient regions. MINet [22] used interactive learning to integrate features from different adjacency levels to preserve the spatial consistency of the predictions. ICON [18] used three diverse aggregations and part-whole verification. EDN [13] focused on the high-level semantic features and proposed an extreme down-sampling method to learn high-level features and recover local details.

Leveraging auxiliary labels is another direction for developing SOD models. Edge map is one of the most used secondary labels in SOD. PoolNet [15] applied a multi-level model to incorporate edge supervision into different stages. EGNNet [34] progressively fused the extracted salient object features with the edge features at various resolutions. Beyond edge maps, LDF [35] decoupled the saliency mask into a body map and a detailed map and learned the two maps with an interactive flow. BiconNet [25] converted the saliency mask into a connectivity mask and proposed a bilateral connectivity learning scheme to model the inter-pixel relationship between neighboring pixels to enhance spatial coherence.

### 2.2. Camouflaged Object Detection

As with SOD, current SOTA methods for COD are CNN-based. Inspired by the bio-related nature of COD, several successful methods mimic the human visual system properties. SINet [9] designed a bio-inspired network with a searching module and a locating module to detect the concealed targets. SLSR [36] modeled the specific part of

camouflaged targets to simultaneously localize, segment, and rank concealed objects. PFNet [37] simulated human identification with the distraction mining strategy. SegMaR [38] utilized a multi-scale learning scheme to integrate the segmentation, magnification, and reiteration in a coarse-to-fine manner. ZoomNet [6] mimicked human behavior when observing a vague image by zooming in and out the images via a multi-scale triplet network.

The edge labels are also widely used. BGNet [39] guided the representation learning with edge semantics. BSANet [40] utilized two-stream separated attention modules to highlight the edges of concealed objects. MGL [41] decoupled an image into two task-specific maps for locating the camouflaged objects and extracting their detailed edges. FEDER [42] decomposed the object features into different frequency bands using learnable wavelets and combined them with an auxiliary edge reconstruction flow to enhance detection. Other impactful approaches for COD include frequency domain learning [43], texture-aware learning [44], uncertainty-guided learning [45, 46], and transformer-based model [47].

### 2.3. Loss Functions in SOD and COD

Efficient loss function design is a crucial component of constructing successful SOD and COD models. One potential solution to solve the inherent limitation of BCE loss used in many popular CNN-based methods [15, 33, 34], is to define hard pixels depending on their location or loss response and weight them. Lin *et al.* [48] weighted each pixel dynamically based on the pixels’ single-response and gave the hard pixels higher weights. Wei *et al.* [21] assumed that the cluttered or elongated areas are prone to wrong predictions and gave higher weights to these pixels. Zhou *et al.* [49] gave higher weights to pixels near object boundaries. For COD applications, Pang *et al.* [6] proposed the UAL loss function to reduce individual pixels’ uncertainty by forcing the objectness probability away from 0.5. Yet, these methods either only relied on the single-response of the prediction [6, 48] or the spatial location of the objects [21, 49], but not the mutual pixel response to determine the hard pixels.

Another set of loss functions is the region-based category, in which a group of pixels is considered for each loss calculation. Corresponding lost functions include [18, 28] that maximized the intersection-over-union (IOU) [50] with a soft region-based loss. Zhao *et al.* [20] proposed a soft F-measure loss to maximize the relaxed F-measurement of SOD models. Pang *et al.* [22] proposed a consistency-enhanced loss (CEL) that maximized a Sørensen–Dice [51] like function. MENet [28] proposed an SSIM-based [52] loss function that computed the standard deviation and covariance for pixels and regions of the predicted map.

Finally, we note that improved performance in current SOTA models, such as MENet [28], EDN [13], and ICON

[18], was achieved in part by combining different loss functions rather than using any of them individually. Inspired by these, in Section 6.5, after demonstrating that the proposed SCLoss outperforms other SOTA loss functions in one-on-one comparisons, we show that it is also compatible with other loss functions and, when combined with them, results in overall best outcomes.

## 3. Methodology

### 3.1. Proposed Spatial Coherence Loss

The proposed Spatial Coherence Loss (SCLoss) combines the classic single-response loss function with a mutual response term and a pairwise regularization term:

$$L = \frac{\textit{Single-Respo}}{\textit{Mutual Response + Pairwise Regularization}}, \quad (1)$$

where the single-response term is the standard pixel-wise loss function (i.e., the loss response from a single pixel) of choice. The mutual response term calculates the co-response of two adjacent pixels, and the pairwise regularization term further enhances the spatial coherence in foreground areas. In brief, we penalize or encourage the objectness probability prediction of individual pixels by the performance of their surrounding pixels to enhance the spatial consistency of the final prediction. In the following, we present our proposed default choices for each of these terms in SOD and COD. In Sections 6.2, 6.4, and 7, we discuss the utility of alternative terms, which show consistent performance improvement as compared to their corresponding baseline loss function.

### 3.2. Instantiation

We call a pixel that is  $k$  pixels apart from a given pixel as its  $k^{\text{th}}$ -level adjacent pixel. Then, for pixel  $i$ , the SCLoss is the weighted sum of sub-losses at different adjacency levels:

$$L_i = \sum_{k=1}^K \left(\frac{1}{2}\right)^{k-1} L_i^k, \quad (2)$$

where  $K$  is the maximum adjacency level (i.e., defining a  $(2K + 1) \times (2K + 1)$  patch). For the  $k^{\text{th}}$  level, the loss  $L_i^k$  for pixel  $i$  is defined in the format of Eqn. (1):

$$L_i^k = \frac{1}{N} \sum_{j \in k^{\text{th}}} \frac{L_{\textit{single}}(p_i, n_i)}{L_{\textit{mutual}}(p_i, p_j, n_i, n_j) + \alpha f(p_i, p_j)}, \quad (3)$$

where  $j$  indexes pixels which are the  $k^{\text{th}}$ -level adjacents of pixel  $i$ ,  $p_i$  and  $p_j$  are the predicted objectness probability at each pixel, and  $n_i$  and  $n_j$  are the labels.  $N$  is the total number of the  $k^{\text{th}}$ -level adjacent pixels of  $i$ .  $L_{\textit{single}}$  is the single-response term,  $L_{\textit{mutual}}$  is the mutual response term, and  $f$  is the pairwise regularization term. Scalar  $\alpha$  balances the contributions of the mutual response and pairwise regularization terms (See Section 6.3).

**Single-response term.** Our default choice for SOD and COD tasks is the BCE loss:

$$L_{single}(p_i, n_i) = n_i \log(p_i) + (1 - n_i) \log(1 - p_i). \quad (4)$$

where  $p_i$  is the predicted objectness probability, and  $n_i$  is the label of pixel  $i$ . Other possible choices for this term are discussed in Section 6.2.

**Mutual response term.** Inspired by the bilateral voting in [25], we define this term for two adjacent pixels  $i$  and  $j$  as:

$$L_{mutual}(p_i, p_j, n_i, n_j) = n_i n_j \log(p_i p_j) + (1 - n_i n_j) \log(1 - p_i p_j). \quad (5)$$

This term adds both the inter-pixel relation and pixel location information into the overall loss calculation. In this setting, the determinacies of the surrounding pixels’ predictions play an important role in weighting the current pixel’s loss calculation. When the two adjacent pixels belong to the same class, the weight of one pixel increases as the other pixel gets a more accurate prediction. In other words, the network will draw more attention to the current pixel if its surrounding pixels make accurate predictions. There are two benefits to this: first, the surrounding pixels encourage the network to make a high spatially coherent prediction; second, when there are wrongly predicted or hard region, the mutual response term gives higher weights to the *boundary* of the hard region, which is surrounded by correctly predicted easy pixels, while giving smaller weights to the region’s center to encourage the network to gradually learn transition from easy pixels to the hard pixels (see Fig. 1 and Section 6.6). When the two pixels are not from the same class, i.e., at the edges, a foreground edge pixel’s weight will be increased when: 1) it is wrongly predicted or 2) the adjacent pixel gets correctly predicted. Intuitively, neighboring correctly-predicted background pixels are utilized to encourage the improvement of incorrectly-predicted foreground pixels by increasing cost.

**Pairwise regularization term.** This term further enhances the spatial coherence of the foreground region. Among many possible options studied in Section 6.4, our default choice is the Gaussian function [53, 54]:

$$f(p_i, p_j) = e^{-p_i p_j}, \quad (6)$$

which locally adjusts the weights by the dot product of the predicted objectness probability. We give the highest weights to the current pixel when both pixels in the pair are predicted as foreground to 1) ensure a high spatial coherence in the foreground prediction; 2) minimize the false positive detections.

## 4. Salient Object Detection

### 4.1. Datasets and evaluation metrics

**Dataset:** We used the training part of DUTS [10] dataset, DUT-TR, for training. For the testing, all methods were

evaluated on the following five popular SOD benchmark datasets. ECSSD [55] has 1,000 images in which the foreground objects are semantically meaningful, and both foregrounds and backgrounds are structurally complex. HKU-IS [56] has 4,447 images, most containing multiple scattered salient objects. DUT-OMRON [3] has 5,168 images with relatively complex backgrounds. PASCAL-S [57] is a subset of PASCAL-VOC 2010, containing 850 images. DUTS-TE [10] is the testing part of the DUTS dataset, with 5,019 images.

**Evaluation Criteria:** We assessed SOD models with the Mean Absolute Error (MAE) [30], the F-measure [58], including the adaptive mean ( $F_\beta^{adp}$ ), max ( $F_{max}$ ), weighted ( $F_\beta^w$ ) F-measure [59], the Enhanced-alignment Measure ( $E_m$ ) [60], and the S-measure ( $S_m$ ) [61].

### 4.2. Implementation details

Our experiments were based on seven state-of-the-art SOD models: GCPA [33], MINet [22], ITSD [49], EDN [13], ICON [18] (including ICON-R and ICON-P), and MENet [28]. For [22, 33, 49], we followed the suggested implementation details in corresponding papers, and for the sake of fairness, we used the same settings for retraining SCLoss. For others [13, 18, 28], we directly loaded their official pretrained model to faithfully reproduce the reported outcomes and then finetuned them with our SCLoss for 10 additional epochs. All the experiments were done on PyTorch 1.7.0 [62] and were performed with an NVIDIA GeForce GTX 3090 Ti GPU.

### 4.3. Overall Results

**Quantitative comparison:** Table 1 compares each baseline with a version trained with SCLoss as a simple add-on loss function. The proposed SCLoss version consistently improved all models across all six utilized metrics. Among these metrics, the  $F_\beta^{adp}$  improved most, which suggests that our loss can uniformly highlight the salient object region, implying the highest spatial coherence [25]. Note that adding SCLoss to the most recent SOTA models: MENet [28], ICON-R (ResNet as the backbone), and ICON-P (vision transformer as the backbone) [18], improved their performance for almost all metrics.

**Qualitative comparison:** Fig. 2 demonstrates the impact of adding SCLoss to different models for different scenarios, including detecting small objects, multiple instances, high-contrast objects, and low-contrast object backgrounds. In all challenging cases, adding SCLoss resulted in visually better object detection compared to the corresponding baseline, where the predicted saliency maps are uniformly highlighted, and the boundaries of the targets are more precise and complete.

Table 1. Quantitative comparison of SOD models on OMRON, HKU-IS, ECSSD, PASCAL, and DUT-TE datasets, without and with SCLoss as an add-on to each model’s recommended loss function. The best results for each metric and dataset are in **bold**.

Model	Year	OMRON (5168 images)						HKU-IS (4447 images)						ECSSD (1000 images)						PASCAL (850 images)						DUT-TE (5019 images)					
		$F_{\beta}^{adp}$	MAE	$E_m$	$F_{\beta}^w$	$S_m$	$F_{max}$	$F_{\beta}^{adp}$	MAE	$E_m$	$F_{\beta}^w$	$S_m$	$F_{max}$	$F_{\beta}^{adp}$	MAE	$E_m$	$F_{\beta}^w$	$S_m$	$F_{max}$	$F_{\beta}^{adp}$	MAE	$E_m$	$F_{\beta}^w$	$S_m$	$F_{max}$	$F_{\beta}^{adp}$	MAE	$E_m$	$F_{\beta}^w$	$S_m$	$F_{max}$
GCPA [33]	2020	.731	.061	.849	.716	.829	.799	.901	.030	.950	.891	.921	.937	.919	.035	.921	.904	.927	.945	.833	.062	.849	.820	.862	.877	.814	.039	.888	.819	.890	.887
+ SCLoss		.768	.056	.867	.747	.837	.814	.920	.028	.955	.901	.921	.938	.933	.032	.927	.916	.929	.948	.845	.059	.858	.827	.860	.880	.844	.035	.903	.835	.891	.890
MINet [22]	2020	.763	.053	.870	.751	.842	.819	.916	.026	.956	.908	.926	.943	.926	.035	.924	.911	.925	.947	.842	.067	.865	.822	.857	.882	.837	.035	.902	.840	.893	.895
+ SCLoss		.778	.051	.876	.756	.839	.819	.923	.025	.958	.912	.924	.941	.935	.032	.928	.918	.924	.949	.849	.065	.867	.827	.858	.886	.858	.034	.912	.847	.890	.894
ITSD [49]	2020	.753	.058	.862	.751	.843	.823	.901	.029	.953	.896	.920	.936	.903	.034	.925	.910	.927	.948	.812	.069	.858	.817	.856	.881	.806	.041	.891	.818	.884	.882
+ SCLoss		.769	.053	.871	.758	.844	.826	.911	.029	.954	.899	.918	.935	.924	.033	.930	.914	.925	.948	.834	.069	.858	.822	.854	.879	.829	.038	.901	.830	.885	.885
EDN [13]	2022	.774	.049	.868	.764	.840	.823	.913	.027	.954	.905	.922	.939	.927	.032	.924	.917	.927	.949	.842	.064	.856	.828	.860	.887	.842	.036	.902	.839	.888	.891
+ SCLoss		.781	.048	.872	.767	.840	.823	.920	.027	.955	.907	.921	.939	.933	.031	.925	.920	.927	.949	.852	.062	.860	.833	.859	.888	.851	.036	.905	.843	.887	.890
ICON-R [18]	2022	.772	.057	.870	.761	.844	.825	.910	.029	.952	.902	.920	.939	.928	.032	.929	.918	.929	.950	.845	.066	.861	.828	.860	.888	.838	.037	.902	.837	.889	.892
+ SCLoss		.783	.055	.875	.768	.846	.826	.921	.027	.955	.909	.923	.940	.937	.029	.932	.925	.932	.952	.851	.064	.863	.831	.861	.886	.852	.036	.907	.843	.890	.891
MENet [28]	2023	.790	.046	.881	.771	.850	.834	.925	.023	.960	.917	.927	.948	.932	.031	.925	.920	.928	.955	.863	.057	.866	.843	.868	.901	.873	.028	.921	.870	.905	.913
+ SCLoss		.796	.047	.881	.781	.855	.839	.932	.022	.963	.925	.933	.951	.941	.027	.931	.931	.936	.960	.868	.057	.867	.848	.870	.899	.877	.028	.921	.875	.909	.913
ICON-P [18]	2022	.794	.047	.886	.793	.865	.852	.925	.022	.963	.925	.935	.952	.936	.024	.928	.933	.940	.959	.867	.052	.873	.857	.881	.906	.868	.026	.919	.882	.917	.922
+ SCLoss		<b>.811</b>	<b>.045</b>	<b>.893</b>	<b>.805</b>	<b>.870</b>	<b>.852</b>	<b>.938</b>	<b>.020</b>	<b>.966</b>	<b>.932</b>	<b>.940</b>	<b>.955</b>	<b>.947</b>	<b>.022</b>	<b>.933</b>	<b>.940</b>	<b>.944</b>	<b>.963</b>	<b>.884</b>	<b>.048</b>	<b>.883</b>	<b>.871</b>	<b>.888</b>	<b>.913</b>	<b>.892</b>	<b>.024</b>	<b>.930</b>	<b>.895</b>	<b>.923</b>	<b>.925</b>

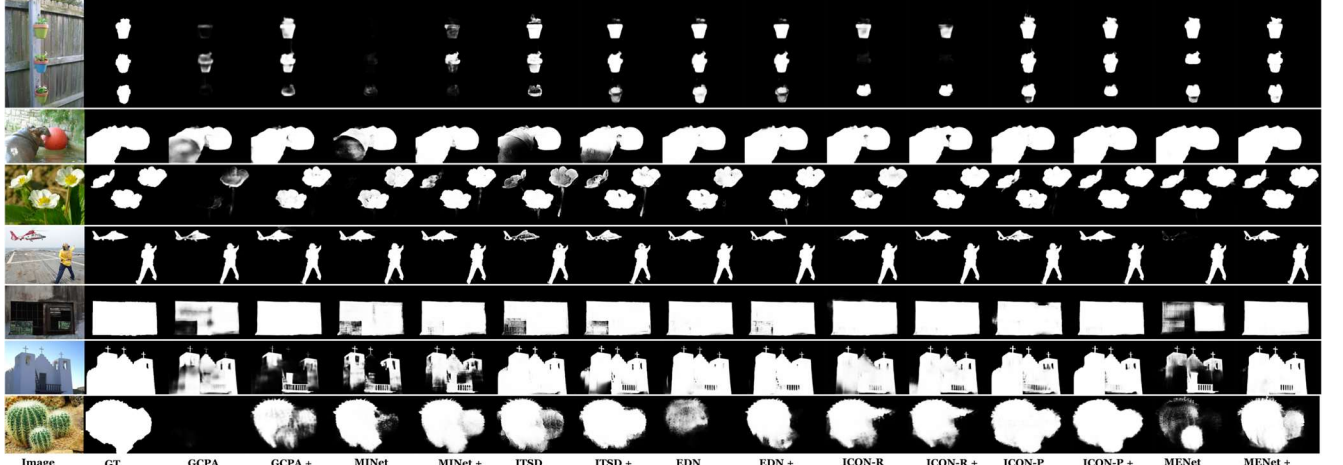


Figure 2 Qualitative comparison between different SOD models trained with/without SCLoss as an add-on to each model’s recommended loss function.

## 5. Camouflaged Object Detection

### 5.1. Datasets and evaluation metrics

**Dataset:** We followed the popular setting in [9] and used the mix of the training part of CAMO [63] and COD10K [9] as the training dataset. For the testing dataset, we used four popular COD datasets: CAMO [63], CHAMELEON [64], COD10K [9], and NC4K [36]. CAMO is a large-scale COD dataset, containing 1,250 camouflaged images and 1,250 non-camouflaged images. CHAMELEON is a smaller dataset that only contains 76 hand-annotated images collected online. COD10K is currently the largest COD dataset, which contains 5,066 camouflaged, 3,000 background, and 1,934 non-camouflaged images. NC4K is another recently released large-scale COD testing dataset that contains 4,121 images.

**Evaluation Criteria:** We used eight evaluation metrics used in [9], including MAE, adaptive F-measure ( $F_{\beta}^{adp}$ ),

weighted F-measure ( $F_{\beta}^w$ ) [59], max F-measure ( $F_{max}$ ), adaptive E-measure ( $E_{\phi}^{adp}$ ) [60], mean E-measure ( $E_{\phi}^m$ ), max E-measure ( $E_{\phi}^x$ ), and S-measure ( $S_m$ ) [61].

### 5.2. Implementation details

Our experiments were based on six state-of-the-art SOD models: GCPA [33], SLSR [36], BGNNet [39], SINet-v2 [65], FEDER [42], and FSPNet [47]. We followed the Section 4.2 implementation details.

### 5.3. Overall Results

**Quantitative comparison:** Table 2 shows the impact of adding SCLoss to the baseline models. SCLoss improved the performance of all models across almost all eight metrics. This includes improving the SOTA results from the most recent models, FEDER [42] and FSPNet [47].

**Qualitative comparison:** Fig. 3 showcases a few challenging scenes for comparison, including camouflaged objects of different sizes and backgrounds. For each model,

Table 2. Quantitative comparison of COD models on CAMO, CHAMELEON, COD10K, and NC4K datasets, without and with SCLoss as an add-on to each model’s recommended loss function. The best results in each metric and dataset are in **bold**.

		CAMO (250 images)							CHAMELEON (67 images)							COD10K (2026 images)							NC4K (4121 images)										
Model	Year	MAE	$F_{\beta}^{adp}$	$F_{\beta}^w$	$F_{max}$	$E_{\phi}^{adp}$	$E_{\phi}^m$	$E_{\phi}^x$	$S_m$	MAE	$F_{\beta}^{adp}$	$F_{\beta}^w$	$F_{max}$	$E_{\phi}^{adp}$	$E_{\phi}^m$	$E_{\phi}^x$	$S_m$	MAE	$F_{\beta}^{adp}$	$F_{\beta}^w$	$F_{max}$	$E_{\phi}^{adp}$	$E_{\phi}^m$	$E_{\phi}^x$	$S_m$	MAE	$F_{\beta}^{adp}$	$F_{\beta}^w$	$F_{max}$	$E_{\phi}^{adp}$	$E_{\phi}^m$	$E_{\phi}^x$	$S_m$
GCPA [33]	2020	.089	.721	.651	.745	.848	.805	.855	.787	.049	.757	.722	.821	.881	.866	.923	.863	.046	.590	.581	.701	.788	.816	.884	.792	.058	.742	.703	.791	.866	.854	.898	.830
+ SCLoss		.086	.741	.660	.740	.848	.800	.847	.782	.035	.799	.766	.835	.911	.900	.946	.871	.041	.641	.612	.701	.829	.825	.884	.786	.054	.774	.721	.791	.884	.859	.898	.825
SLSR [36]	2021	.084	.759	.691	.757	.863	.836	.862	.785	.033	.811	.802	.855	.924	.933	.954	.881	.039	.675	.655	.726	.860	.869	.890	.802	.054	.778	.739	.799	.891	.881	.901	.831
+ SCLoss		.080	.764	.701	.769	.867	.850	.870	.795	.032	.823	.810	.861	.932	.935	.950	.882	.037	.686	.667	.733	.871	.881	.896	.806	.051	.784	.748	.805	.895	.889	.903	.833
SINet-v2 [65]	2022	.070	.779	.743	.801	.885	.882	.895	.820	.030	.816	.816	.867	.929	.941	.961	.888	.037	.682	.680	.752	.864	.887	.906	.815	.048	.792	.769	.823	.901	.902	.913	.847
+ SCLoss		.069	.789	.749	.805	.890	.883	.896	.823	.028	.829	.823	.869	.937	.943	.963	.891	.035	.696	.688	.754	.875	.891	.907	.817	.047	.799	.772	.823	.905	.902	.914	.847
BGNet [39]	2022	.075	.778	.736	.789	.860	.852	.865	.803	.028	.838	.840	.873	.934	.939	.953	.896	.032	.738	.719	.770	.901	.897	.908	.830	.045	.813	.786	.830	.909	.901	.912	.851
+ SCLoss		.069	.791	.753	.806	.879	.875	.886	.815	.028	.846	.847	.879	.939	.948	.960	.898	.031	.740	.721	.772	.901	.898	.908	.831	.044	.817	.790	.833	.911	.905	.915	.852
FEDER [42]	2023	.076	.768	.715	.767	.862	.850	.862	.785	.029	.848	.836	.870	.946	.949	.956	.887	.033	.732	.707	.757	.901	.896	.902	.817	.046	.812	.777	.822	.907	.899	.906	.841
+ SCLoss		.072	.784	.737	.789	.877	.869	.876	.803	.027	.848	.840	.870	.947	<b>.951</b>	.958	.890	.032	.735	.715	.768	.898	.901	.908	.824	.044	.820	.789	.833	.914	.909	.916	.849
FSPNet [47]	2023	.051	.828	.799	.853	.919	.899	.928	.856	.025	.845	.839	.885	.944	.938	.965	.904	.027	.729	.732	.797	.896	.894	.930	<b>.851</b>	.035	.823	.816	.861	.922	.915	.937	<b>.878</b>
+ SCLoss		<b>.049</b>	<b>.836</b>	<b>.810</b>	<b>.854</b>	<b>.921</b>	<b>.908</b>	<b>.929</b>	<b>.858</b>	<b>.022</b>	<b>.873</b>	<b>.855</b>	<b>.890</b>	<b>.962</b>	.946	<b>.968</b>	<b>.904</b>	<b>.026</b>	<b>.753</b>	<b>.742</b>	<b>.798</b>	<b>.908</b>	<b>.899</b>	<b>.931</b>	.847	<b>.035</b>	<b>.836</b>	<b>.823</b>	<b>.864</b>	<b>.926</b>	<b>.920</b>	<b>.939</b>	.877

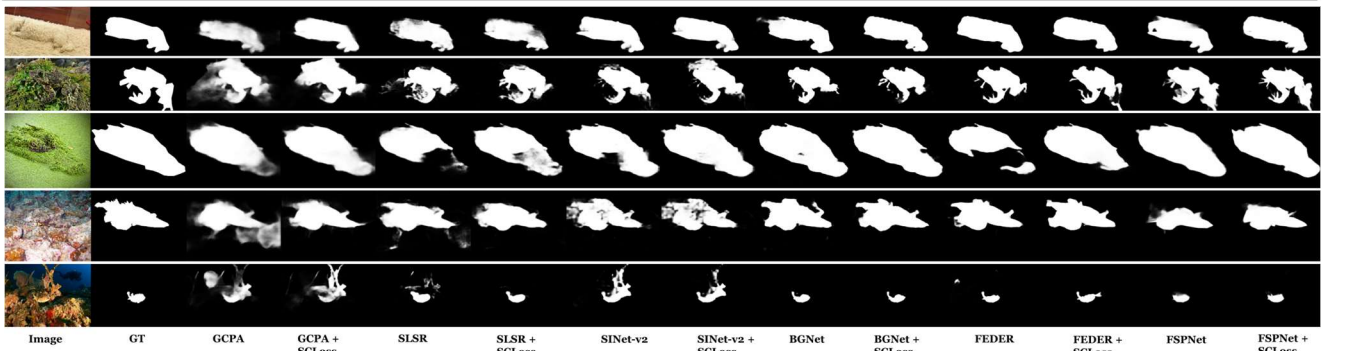


Figure 3. Comparison between different COD models trained with/without SCLoss as an add-on to each model’s recommended loss function.

Table 3. Ablation study on the adjacency levels for SCLoss in SOD (Top) and COD (Down). The training GPU memory costs on are also reported.

		SOD - ECSSD					SOD - HKU-IS					SOD - OMRON					SOD - PASCAL					SOD - DUT-TE								
Exp.	$F_{max}$	$F_{\beta}^{adp}$	MAE	$F_{\beta}^w$	$S_m$	$E_m$	$F_{max}$	$F_{\beta}^{adp}$	MAE	$F_{\beta}^w$	$S_m$	$E_m$	$F_{max}$	$F_{\beta}^{adp}$	MAE	$F_{\beta}^w$	$S_m$	$E_m$	$F_{max}$	$F_{\beta}^{adp}$	MAE	$F_{\beta}^w$	$S_m$	$E_m$	$F_{max}$	$F_{\beta}^{adp}$	MAE	$F_{\beta}^w$	$S_m$	$E_m$
GCPA	.945	.919	.035	.904	.927	.921	.937	.901	.030	.891	.921	.950	.799	.731	.061	.716	.829	.849	.877	.833	.062	.820	.862	.849	.887	.814	.039	.819	.890	.888
K=1	.947	.930	.033	.912	.927	.927	.936	.912	.030	.897	.919	.952	.803	.754	.055	.732	.830	.866	.877	.842	.060	.824	.859	.854	.887	.837	.036	.829	.888	.903
K=2	.948	.933	.032	.916	.929	.927	.938	.920	.028	.901	.921	.955	.814	.768	.056	.747	.837	.867	.880	.845	.059	.827	.860	.858	.890	.844	.035	.835	.891	.903
K=3	.948	.930	.033	.914	.927	.927	.936	.916	.029	.898	.918	.954	.808	.760	.055	.740	.832	.866	.877	.845	.059	.824	.857	.864	.889	.846	.035	.834	.889	.907

		COD - CAMO					COD - CHAMELEON					COD - COD10K					COD - NC4K					Training Memory (GB)							
Exp.	$S_m$	$F_{\beta}^w$	MAE	$E_{\phi}^{adp}$	$E_{\phi}^m$	$E_{\phi}^x$	$F_{\beta}^{adp}$	$S_m$	$F_{\beta}^w$	MAE	$E_{\phi}^{adp}$	$E_{\phi}^m$	$E_{\phi}^x$	$F_{\beta}^{adp}$	$S_m$	$F_{\beta}^w$	MAE	$E_{\phi}^{adp}$	$E_{\phi}^m$	$E_{\phi}^x$	$F_{\beta}^{adp}$	$S_m$	$F_{\beta}^w$	MAE	$E_{\phi}^{adp}$	$E_{\phi}^m$	$E_{\phi}^x$	$F_{\beta}^{adp}$	
SLSR	.785	.691	.084	.863	.836	.862	.759	.881	.802	.033	.924	.933	.954	.811	.802	.655	.039	.860	.869	.890	.675	.831	.739	.054	.891	.881	.901	.778	7.6
K=1	.787	.696	.083	.863	.838	.859	.759	.882	.804	.033	.928	.935	.953	.812	.805	.662	.038	.864	.879	.896	.677	.833	.746	.052	.894	.887	.903	.780	9.3
K=2	.795	.701	.080	.867	.850	.870	.764	.882	.810	.032	.932	.935	.950	.823	.806	.667	.037	.871	.881	.896	.686	.833	.748	.051	.895	.889	.903	.784	11.2
K=3	.790	.700	.082	.865	.844	.867	.760	.880	.807	.033	.931	.934	.952	.823	.805	.668	.037	.871	.881	.897	.688	.832	.748	.052	.895	.888	.904	.785	13.0

adding SCLoss resulted in visually more acceptable detection compared to the baseline. Particularly, our results have fewer false positive predictions, higher confidence, and more precise predictions in the foreground objects.

## 6. Ablation Study

To study the impact of each SCLoss component, we used two widely used baselines GCPA [33] and SLSR [36], for the SOD and COD experiments, respectively.

### 6.1. Adjacency Level of SCLoss

We first study the impact of the maximum adjacency level  $K$  in Eqn. (2) on SCLoss. Table 3 shows the

improvements gained by adding SCLoss with the total level  $K$  of 1, 2, and 3 to baseline models. The GPU-memory cost as a function of  $K$  in the training phase is listed in the last column of Table 3. Comparison of the baseline with the case of  $K = 1$ , shows that incorporating even the simplest form of the SCLoss into the training, greatly improves the baseline performance. Increasing the adjacency level ( $K = 2$ ), further improves the performance, but performance improvements are saturated at higher  $K$  values (which also have slightly higher memory costs in the training process). Thus, we set  $K = 2$  as our default choice for the best balance of performance and GPU-memory cost.

Table 4. Ablation Study on selection of  $L_{single}$ . We used two other common single-response based losses, MSE and L1 loss as our baselines and established SCLoss on each of them for SOD and COD experiments.

Loss	SOD - GCPA - ECSSD				SOD - GCPA - HKU-IS				COD - SLSR - CAMO					COD - SLSR - NC4K								
	$F_{\beta}^{adv}$	MAE	$S_m$	$E_m$	$F_{\beta}^{adv}$	MAE	$S_m$	$E_m$	$S_m$	$F_{\beta}^w$	MAE	$E_{\phi}^{adv}$	$E_{\phi}^m$	$E_{\phi}^x$	$F_{\beta}^{adv}$	$S_m$	$F_{\beta}^w$	MAE	$E_{\phi}^{adv}$	$E_{\phi}^m$	$E_{\phi}^x$	$F_{\beta}^{adv}$
L1 Loss	.924	.033	.915	.918	.912	.028	.910	.950	.753	.666	.084	.836	.814	.846	.741	.796	.718	.055	.879	.859	.886	.779
L1 SCLoss	.931	.032	.915	.920	.919	.027	.907	.947	.775	.711	.078	.859	.854	.861	.763	.810	.744	.052	.889	.885	.890	.785
MSE Loss	.882	.044	.922	.919	.887	.039	.917	.945	.785	.645	.090	.851	.798	.865	.728	.817	.680	.063	.860	.835	.896	.735
MSE SCLoss	.924	.037	.923	.924	.911	.032	.917	.952	.784	.677	.080	.876	.821	.878	.765	.816	.713	.056	.883	.856	.900	.772

Table 5. Ablation Study on selection of  $\alpha$ . Due to limited space, we used one dataset from each task to compare the impact of  $\alpha = 0.5, 1, \text{ and } 2$ .

Exp.	SOD - GCPA - ECSSD							COD - SLSR - CAMO						
	$F_{\max}$	$F_{\beta}^{adv}$	MAE	$F_{\beta}^w$	$S_m$	$E_m$	$S_m$	$F_{\beta}^w$	MAE	$E_{\phi}^{adv}$	$E_{\phi}^m$	$E_{\phi}^x$	$F_{\beta}^{adv}$	
$\alpha=0.5$	.946	.933	.032	.913	.926	.926	.792	.704	.083	.861	.848	.862	.759	
$\alpha=1$	.948	.933	.032	.916	.929	.927	.795	.701	.080	.867	.850	.870	.764	
$\alpha=2$	.946	.928	.035	.908	.925	.923	.785	.693	.084	.864	.836	.862	.758	

## 6.2. Selection of Single-response Term

The choice for  $L_{single}$  depends on the task at hand. Table 4 shows the impact of using two (alternative to BCE) widely used single-response loss functions, MSE loss and L1 loss. We compared the performance of GCPA for SOD and SLSR for COD tasks, when using MSE or L1 or their SCLoss version as the loss function. In the latter SCLoss case, MSE or L1 were used as the single-response term in Eqn. (3). The consistent improvements gained by using the SCLoss version of these loss functions suggest that other single-response terms may also benefit from our proposed loss scheme in Eqn. (1).

## 6.3. Impact of $\alpha$

Table 5 assesses the impact of the mutual response and pairwise regularization terms in SCLoss by comparing the performance of the SCLoss-enhanced GCPA and SLSR with  $\alpha = 0.5, 1, \text{ and } 2$ . A lower value of  $\alpha$  indicates that the weight will depend more on the mutual response between the pixel pairs and vice versa. The best experimental results were achieved with  $\alpha = 1$ . Increasing  $\alpha$  to 2 lowered the performance. These experiments emphasized the importance of using both terms together to achieve optimal outcomes.

## 6.4. Selection of Pairwise Regularization Term

In Section 3.2, we chose the Gaussian function as the default pairwise regularization term. Table 6 compares the performance of other options (among many) for this term.

**Constant regularization.**  $f(p_i, p_j) = 1$ , is the simplest option to avoid overflow in loss back-propagation, and as expected, it did not result in the best performance.

**Distance regularization,** in the form of the Euclidean distance [53], is defined as:

$$f(p_i, p_j) = e^{(p_i - p_j)^2}. \quad (8)$$

Compared to the Gaussian regularization in Eqn. (6), this function gives the largest weight when  $p_1 = p_2$ , which

Table 6. Ablation Study on the choice for pairwise regularization term.

Exp.	SOD - GCPA - ECSSD						COD - SLSR - CHAMELEON						
	$F_{\max}$	$F_{\beta}^{adv}$	MAE	$F_{\beta}^w$	$S_m$	$E_m$	$S_m$	$F_{\beta}^w$	MAE	$E_{\phi}^{adv}$	$E_{\phi}^m$	$E_{\phi}^x$	$F_{\beta}^{adv}$
Constant	.947	.929	.033	.912	.927	.922	.876	.802	.033	.929	.925	.937	.817
Distance	.950	.931	.033	.916	.928	.926	.883	.805	.033	.928	.934	.951	.814
Gaussian	.948	.933	.032	.916	.929	.927	.882	.810	.032	.932	.935	.950	.823

ensures a smooth and polarized prediction [6, 20]. However, it gives less regularization when there is a likely edge prediction. On the other hand, Eqn. (6) is maximized in cases where both predictions are close to 1, while giving moderate weight to the potential edge predictions. Thus, it reduces the false positives to achieve low MAE and results in predictions with high spatial coherence.

## 6.5. Loss Comparison and Compatibility Study

**Loss Comparison.** While re-emphasizing that SCLoss can be utilized in combination with previously proposed cost functions, for the sake of completeness, Table 7 compares the one-to-one performance of SCLoss and other popular loss functions in SOD and COD. Specifically, we report the performance of GCPANet (SOD) and SLSR (COD) as the backbones using either of the proposed SCLoss, BCE loss, CEL [22], Structure Loss [21], F-loss [20], or UAL [6]. In these one-to-one comparisons, SCLoss produced the overall best results. Compared to F-loss, SCLoss achieved much better results on metrics MAE,  $S_m$ , and E-measures. Compared to all other losses, SCLoss produced the best MAE, F-measures, and E-measures.

**Compatibility Study.** Even more encouraging than the one-to-one comparisons, Table 8 shows the compatibility of SCLoss when combined with other loss functions. Following [28], our experiments were based on two SOTA models (ICON [18] and MENet [28]) in SOD by gradually adding different loss functions in these two papers to the models. Noticeably, adding SCLoss to the already complex loss functions improved the models' performance.

## 6.6. Gradual Learning Process of Hard Regions

Fig. 4 visualizes the learning process of SCLoss when dealing with hard regions. In Fig. 4(c), we show the predictions of a specific image, Fig. 4(a), in the training process. To visualize how SCLoss gave attention to the boundary of the hard regions and gradually learned the hard pixels, Fig. 4(d) shows the corresponding weight attention map of the SCLoss, i.e., one over the denominator of Eqn. (3). At earlier epochs, when the network could not

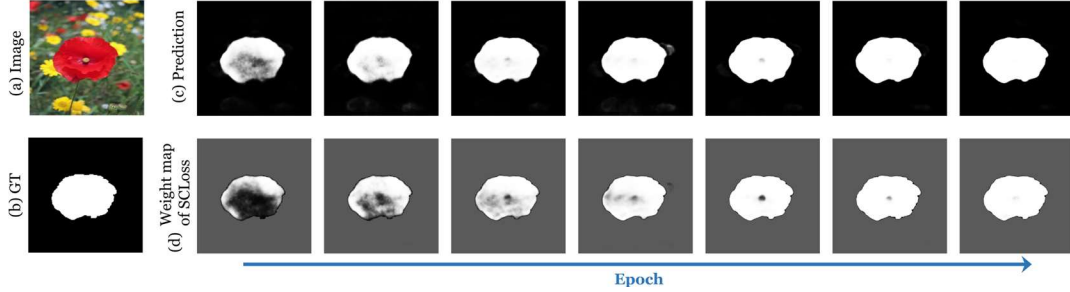


Figure 4. Visualization of the gradual learning process of an example hard region (i.e., the pistil region) in image (a). Image series (c) are the predictions of the model at different epochs. (d) are the corresponding weight attention maps produced by SCLoss.

Table 7. Comparison between SCLoss and other loss functions in SOD and COD tasks. GCPA was used for SOD and SLSR was used for COD.

Loss	SOD - GCPA - ECSSD				SOD - GCPA - PASCAL				SOD - GCPA - DUT-TE				COD - SLSR - CAMO						COD - SLSR - NC4K							
	$F_{\beta}^{adp}$	MAE	$S_m$	$E_m$	$F_{\beta}^{adp}$	MAE	$S_m$	$E_m$	$F_{\beta}^{adp}$	MAE	$S_m$	$E_m$	$S_m$	$F_{\beta}^w$	MAE	$E_{\phi}^{adp}$	$E_{\phi}^m$	$E_{\phi}^x$	$F_{\beta}^{adp}$	$S_m$	$F_{\beta}^w$	MAE	$E_{\phi}^{adp}$	$E_{\phi}^m$	$E_{\phi}^x$	$F_{\beta}^{adp}$
BCE	.919	.035	.927	.921	.833	.062	.862	.849	.814	.039	.890	.888	.788	.649	.089	.857	.797	.863	.737	.821	.684	.061	.867	.835	.897	.745
CEL [22]	.923	.033	.926	.921	.836	.063	.856	.846	.829	.037	.889	.896	.787	.684	.082	.870	.832	.870	.752	.822	.722	.055	.885	.866	.896	.768
Structure [21]	.926	.032	.927	.923	.841	.061	.858	.848	.841	.036	.892	.902	.785	.691	.084	.863	.836	.862	.759	.831	.739	.054	.891	.881	.901	.778
F-Loss [20]	.937	.033	.914	.923	.854	.062	.844	.852	.863	.038	.864	.897	.758	.690	.084	.842	.829	.855	.766	.798	.733	.056	.884	.873	.892	.794
UAL [6]	.927	.032	.925	.924	.839	.059	.855	.852	.842	.036	.886	.901	.783	.691	.080	.867	.837	.868	.761	.824	.734	.053	.891	.873	.899	.782
SCLoss	.933	.032	.929	.927	.845	.059	.860	.858	.844	.035	.891	.903	.795	.701	.080	.867	.850	.870	.764	.833	.748	.051	.895	.889	.903	.784

Table 8. SCLoss Compatibility study. In each row, we add more losses to two SOTA SOD models (MENet [28] and ICON-P [18]). By adding SCLoss, both models were improved, achieving new SOTA results.

Model	Loss	OMRON				HKU-IS				DUT-TE			
		$F_{\beta}^{adp}$	MAE	$S_m$	$E_m$	$F_{\beta}^{adp}$	MAE	$S_m$	$E_m$	$F_{\beta}^{adp}$	MAE	$S_m$	$E_m$
MENet	+ BCE	.778	.052	.841	.868	.913	.024	.927	.960	.858	.031	.899	.908
	+ $L_g + L_s$	.790	.046	.850	.881	.925	.023	.927	.960	.873	.028	.905	.921
	+ SCLoss	.796	.047	.855	.881	.932	.022	.933	.963	.877	.028	.909	.921
ICON-P	+ BCE	.785	.050	.861	.881	.916	.023	.933	.960	.860	.026	.917	.913
	+ IoU	.794	.047	.865	.886	.925	.022	.935	.963	.868	.026	.917	.919
	+ SCLoss	.811	.045	.870	.893	.938	.020	.940	.966	.892	.024	.923	.930

accurately capture the texture of the flower, the SCLoss emphasized most on the petals. Then, the network gradually gave more attention to the hardest part of the image – the pistil. The network attention started with the intersection of the petal and the pistil, rather than the center of the pistil, to learn the transition between the learned easy regions (petal) and the unlearned hard regions (pistil) and gradually moved to the center of the pistil. Eventually, the network produced a perfect detection of the flower.

## 7. Potential on Other Fields

Given its promising results for generic object detection, we expect that the proposed SCLoss can be impactful in many other computer vision tasks, including but not limited to semantic segmentation [66], pose estimation [67], medical image analysis [68], knowledge distillation [69], etc. While a comprehensive study of all the applications is out of the scope of this paper, for the sake of completeness, we show the utility of SCLoss for semantic segmentation.

**Semantic segmentation** experiments were based on two widely used semantic segmentation datasets, CamVid [70] and PASCAL-VOC [71]. We followed the same setting in

Table 9. SCLoss for semantic segmentation. The experiments were conducted on CamVid and PASCAL-VOC datasets.

Method	Val ACC (%)	Val mIoU (%)	Test ACC (%)	Test mIoU (%)	
	DeepLab V3 - Res18	95.19	76.53	91.78	66.92
+SCLoss	95.35	77.71	92.19	68.91	
DeepLab V3 - Res101	95.40	77.95	92.53	69.84	
+ SCLoss	95.85	79.65	92.60	70.55	
PASCAL-VOC	DeepLab V3 - Res18	93.80	73.60		
	+SCLoss	94.58	74.74		
	DeepLab V3 - Res101	94.99	77.04		
+ SCLoss	94.99	77.98			

[69] to train the baselines on DeepLab V3 [66] and assessed the impact of adding SCLoss to the baseline model. For the multi-class setting, we used cross entropy as the single-response term  $L_{single}$ . Table 9 shows adding SCLoss improves performance in all cases attesting to its potential for applications in other fields.

## 8. Conclusion

This paper introduced a novel loss scheme, SCLoss, for generic object detection. We proposed that utilizing the mutual response between pixels can enhance the spatial coherence of generic object detection. We investigated the utility of proposed SCLoss by conducting comprehensive experiments on two tasks, SOD and COD. We showed the effectiveness of incorporating SCLoss with the SOTA models as backbones and achieved the new SOTA results on both tasks. The proposed SCLoss was compatible with other loss functions and improved performance when added to existing models. SCLoss was robust with respect to the choice of its individual components, such as the single-response term. We showed the results of a semantic segmentation task as a demonstrative example of the potential utility of SCLoss in other related tasks, such as medical image analysis and knowledge distillation.



## References

- [1] B. Xiong, S. D. Jain, and K. Grauman, "Pixel Objectness: Learning to Segment Generic Objects Automatically in Images and Videos," *IEEE TPAMI*, vol. 41, no. 11, pp. 2677-2692, 2019.
- [2] P. T. Jiang, L. H. Han, Q. Hou, M. M. Cheng, and Y. Wei, "Online Attention Accumulation for Weakly Supervised Semantic Segmentation," *IEEE TPAMI*, vol. 44, no. 10, pp. 7062-7077, 2022.
- [3] C. Yang, L. Zhang, H. Lu, X. Ruan, and M.-H. Yang, "Saliency detection via graph-based manifold ranking," in *CVPR*, 2013, pp. 3166-3173.
- [4] Y. Gao, M. Wang, Z. J. Zha, J. Shen, X. Li, and X. Wu, "Visual-Textual Joint Relevance Learning for Tag-Based Social Image Search," *IEEE TIP*, vol. 22, no. 1, pp. 363-376, 2013.
- [5] P. L. Rosin and Y.-K. Lai, "Artistic minimal rendering with lines and blocks," *Graphical Models*, vol. 75, no. 4, pp. 208-229, 2013.
- [6] Y. Pang, X. Zhao, T. Z. Xiang, L. Zhang, and H. Lu, "Zoom In and Out: A Mixed-scale Triplet Network for Camouflaged Object Detection," in *CVPR*, 2022, pp. 2150-2160.
- [7] L.-C. Chen, Y. Zhu, G. Papandreou, F. Schroff, and H. Adam, "Encoder-Decoder with Atrous Separable Convolution for Semantic Image Segmentation," in *ECCV*, 2018, pp. 833-851.
- [8] Z. Yang and S. Farsiu, "Directional Connectivity-based Segmentation of Medical Images," in *CVPR*, 2023, pp. 11525-11535.
- [9] D. P. Fan, G. P. Ji, G. Sun, M. M. Cheng, J. Shen, and L. Shao, "Camouflaged Object Detection," in *CVPR*, 2020, pp. 2774-2784.
- [10] L. Wang et al., "Learning to detect salient objects with image-level supervision," in *CVPR*, 2017, pp. 136-145.
- [11] N. Liu, J. Han, and M. Yang, "PiCANet: Learning Pixel-Wise Contextual Attention for Saliency Detection," in *CVPR*, 2018, pp. 3089-3098.
- [12] P. Zhang, D. Wang, H. Lu, H. Wang, and X. Ruan, "Amulet: Aggregating multi-level convolutional features for salient object detection," in *ICCV*, 2017, pp. 202-211.
- [13] Y. H. Wu, Y. Liu, L. Zhang, M. M. Cheng, and B. Ren, "EDN: Salient Object Detection via Extremely-Downsampled Network," *IEEE TIP*, vol. 31, pp. 3125-3136, 2022.
- [14] Y. Zeng, P. Zhang, Z. Lin, J. Zhang, and H. Lu, "Towards High-Resolution Salient Object Detection," in *ICCV*, 2019, pp. 7233-7242.
- [15] J.-J. Liu, Q. Hou, M.-M. Cheng, J. Feng, and J. Jiang, "A simple pooling-based design for real-time salient object detection," in *CVPR*, 2019, pp. 3917-3926.
- [16] Q. Zhang et al., "Dense Attention Fluid Network for Salient Object Detection in Optical Remote Sensing Images," *IEEE TIP*, vol. 30, pp. 1305-1317, 2021.
- [17] T. Zhao and X. Wu, "Pyramid Feature Attention Network for Saliency Detection," in *CVPR*, 2019, pp. 3080-3089.
- [18] M. Zhuge, D. P. Fan, N. Liu, D. Zhang, D. Xu, and L. Shao, "Salient Object Detection via Integrity Learning," *IEEE TPAMI*, vol. 45, no. 3, pp. 3738-3752, 2023.
- [19] P.-T. De Boer, D. P. Kroese, S. Mannor, and R. Y. J. A. o. o. r. Rubinstein, "A tutorial on the cross-entropy method," *Ann. Oper. Res.*, vol. 134, no. 1, pp. 19-67, 2005.
- [20] K. Zhao, S. Gao, W. Wang, and M.-M. Cheng, "Optimizing the f-measure for threshold-free salient object detection," in *ICCV*, 2019, pp. 8849-8857.
- [21] J. Wei, S. Wang, and Q. Huang, "F<sup>3</sup>Net: fusion, feedback and focus for salient object detection," in *AAAI*, 2020, vol. 34, no. 07, pp. 12321-12328.
- [22] Y. Pang, X. Zhao, L. Zhang, and H. Lu, "Multi-Scale Interactive Network for Salient Object Detection," in *CVPR*, 2020, pp. 9413-9422.
- [23] B. Li, Y. Liu, and X. Wang, "Gradient harmonized single-stage detector," in *AAAI*, 2019, vol. 33, no. 01, pp. 8577-8584.
- [24] M. Kampffmeyer, N. Dong, X. Liang, Y. Zhang, and E. P. Xing, "ConnNet: A long-range relation-aware pixel-connectivity network for salient segmentation," *IEEE TIP*, vol. 28, no. 5, pp. 2518-2529, 2018.
- [25] Z. Yang, S. Soltanian-Zadeh, and S. Farsiu, "BiconNet: An Edge-preserved Connectivity-based Approach for Salient Object Detection," *Pattern Recognit.*, vol. 121, p. 108231, 2022.
- [26] M. A. Halko, E. Mingolla, and D. C. Somers, "Multiple mechanisms of illusory contour perception," *Journal of Vision*, vol. 8, no. 11, pp. 17-17, 2008.
- [27] J. W. Peirce, "Understanding mid-level representations in visual processing," *Journal of Vision*, vol. 15, no. 7, pp. 5-5, 2015.
- [28] Y. Wang, R. Wang, X. Fan, T. Wang, and X. He, "Pixels, Regions, and Objects: Multiple Enhancement for Salient Object Detection," in *CVPR*, 2023, pp. 10031-10040.
- [29] R. S. Srivatsa and R. V. Babu, "Salient object detection via objectness measure," in *ICIP*, 2015, pp. 4481-4485.
- [30] F. Perazzi, P. Krähenbühl, Y. Pritch, and A. Hornung, "Saliency filters: Contrast based filtering for salient region detection," in *CVPR*, 2012, pp. 733-740.
- [31] M.-M. Cheng, J. Warrell, W.-Y. Lin, S. Zheng, V. Vineet, and N. Crook, "Efficient salient region detection with soft image abstraction," in *ICCV*, 2013, pp. 1529-1536.
- [32] Q. Hou, M.-M. Cheng, X. Hu, A. Borji, Z. Tu, and P. H. Torr, "Deeply supervised salient object detection with short connections," in *CVPR*, 2017, pp. 3203-3212.
- [33] Z. Chen, Q. Xu, R. Cong, and Q. Huang, "Global context-aware progressive aggregation network for salient object detection," in *AAAI*, 2020, vol. 34, no. 07, pp. 10599-10606.
- [34] J.-X. Zhao, J.-J. Liu, D.-P. Fan, Y. Cao, J. Yang, and M.-M. Cheng, "EGNet: Edge guidance network for salient object detection," in *ICCV*, 2019, pp. 8779-8788.
- [35] J. Wei, S. Wang, Z. Wu, C. Su, Q. Huang, and Q. Tian, "Label Decoupling Framework for Salient Object Detection," in *CVPR*, 2020, pp. 13025-13034.
- [36] Y. Lv et al., "Simultaneously Localize, Segment and Rank the Camouflaged Objects," in *CVPR*, 2021, pp. 11586-11596.
- [37] H. Mei, G. P. Ji, Z. Wei, X. Yang, X. Wei, and D. P. Fan, "Camouflaged Object Segmentation with Distraction Mining," in *CVPR*, 2021, pp. 8768-8777.
- [38] Q. Jia, S. Yao, Y. Liu, X. Fan, R. Liu, and Z. Luo, "Segment, Magnify and Reiterate: Detecting Camouflaged Objects the Hard Way," in *CVPR*, 2022, pp. 4703-4712.

- [39] T. Chen, J. Xiao, X. Hu, G. Zhang, and S. Wang, "Boundary-guided network for camouflaged object detection," *Knowledge-Based Systems*, vol. 248, p. 108901, 2022.
- [40] H. Zhu et al., "I Can Find You! Boundary-Guided Separated Attention Network for Camouflaged Object Detection," *AAAI*, vol. 36, no. 3, pp. 3608-3616, 2022.
- [41] Q. Zhai et al., "MGL: Mutual Graph Learning for Camouflaged Object Detection," *IEEE TIP*, vol. 32, pp. 1897-1910, 2023.
- [42] C. He et al., "Camouflaged Object Detection with Feature Decomposition and Edge Reconstruction," in *CVPR*, 2023, pp. 22046-22055.
- [43] Y. Zhong, B. Li, L. Tang, S. Kuang, S. Wu, and S. Ding, "Detecting Camouflaged Object in Frequency Domain," in *CVPR*, 2022, pp. 4494-4503.
- [44] J. Zhu, X. Zhang, S. Zhang, and J. Liu, "Inferring Camouflaged Objects by Texture-Aware Interactive Guidance Network," in *AAAI*, vol. 35, no. 4, pp. 3599-3607, 2021.
- [45] A. Li, J. Zhang, Y. Lv, B. Liu, T. Zhang, and Y. Dai, "Uncertainty-aware Joint Salient Object and Camouflaged Object Detection," in *CVPR*, 2021, pp. 10066-10076.
- [46] J. Liu, J. Zhang, and N. Barnes, "Modeling Aleatoric Uncertainty for Camouflaged Object Detection," in *WACV*, 2022, pp. 2613-2622.
- [47] Z. Huang et al., "Feature Shrinkage Pyramid for Camouflaged Object Detection with Transformers," in *CVPR*, 2023, pp. 5557-5566.
- [48] T. Y. Lin, P. Goyal, R. Girshick, K. He, and P. Dollár, "Focal Loss for Dense Object Detection," in *ICCV*, 2017, pp. 2999-3007.
- [49] H. Zhou, X. Xie, J.-H. Lai, Z. Chen, and L. Yang, "Interactive Two-Stream Decoder for Accurate and Fast Saliency Detection," in *CVPR*, 2020, pp. 9141-9150.
- [50] M. A. Rahman and Y. Wang, "Optimizing Intersection-Over-Union in Deep Neural Networks for Image Segmentation," in *Adv. Vis. Comput.*, 2016, pp. 234-244.
- [51] F. Milletari, N. Navab, and S. Ahmadi, "V-Net: Fully convolutional neural networks for volumetric medical image segmentation," in *3DV*, 2016, pp. 565-571.
- [52] W. Zhou, A. C. Bovik, H. R. Sheikh, and E. P. Simoncelli, "Image quality assessment: from error visibility to structural similarity," *IEEE TIP*, vol. 13, no. 4, pp. 600-612, 2004.
- [53] X. Wang, R. Girshick, A. Gupta, and K. He, "Non-local neural networks," in *CVPR*, 2018, pp. 7794-7803.
- [54] C. Tomasi and R. Manduchi, "Bilateral filtering for gray and color images," in *ICCV*, 1998, pp. 839-846.
- [55] Q. Yan, L. Xu, J. Shi, and J. Jia, "Hierarchical saliency detection," in *CVPR*, 2013, pp. 1155-1162.
- [56] G. Li and Y. Yu, "Visual saliency based on multiscale deep features," in *CVPR*, 2015, pp. 5455-5463.
- [57] Y. Li, X. Hou, C. Koch, J. M. Rehg, and A. L. Yuille, "The secrets of salient object segmentation," in *CVPR*, 2014, pp. 280-287.
- [58] R. Achanta, S. Hemami, F. Estrada, and S. Susstrunk, "Frequency-tuned salient region detection," in *CVPR*, 2009, pp. 1597-1604.
- [59] R. Margolin, L. Zelnik-Manor, and A. Tal, "How to Evaluate Foreground Maps," in *CVPR*, 2014, pp. 248-255.
- [60] D.-P. Fan, C. Gong, Y. Cao, B. Ren, M.-M. Cheng, and A. Borji, "Enhanced-alignment measure for binary foreground map evaluation," in *IJCAI*, 2018, pp. 698-704.
- [61] D.-P. Fan, M.-M. Cheng, Y. Liu, T. Li, and A. Borji, "Structure-measure: A new way to evaluate foreground maps," in *ICCV*, 2017, pp. 4548-4557.
- [62] A. Paszke et al., "Pytorch: An imperative style, high-performance deep learning library," in *NIPS*, 2019, pp. 8026-8037.
- [63] T.-N. Le, T. V. Nguyen, Z. Nie, M.-T. Tran, and A. Sugimoto, "Anabranch network for camouflaged object segmentation," *Comput. Vis. Image Underst.*, vol. 184, pp. 45-56, 2019.
- [64] P. Skurowski, H. Abdulameer, J. Błaszczyk, T. Depta, A. Kornacki, and P. Koziel, "Animal camouflage analysis: Chameleon database," *Unpublished manuscript*, 2018.
- [65] D. P. Fan, G. P. Ji, M. M. Cheng, and L. Shao, "Concealed Object Detection," *IEEE TPAMI*, vol. 44, no. 10, pp. 6024-6042, 2022.
- [66] L.-C. Chen, G. Papandreou, F. Schroff, and H. J. A. Adam, "Rethinking Atrous Convolution for Semantic Image Segmentation," *arXiv preprint arXiv:1706.05587*, 2017.
- [67] T. Lee et al., "UDA-COPE: Unsupervised Domain Adaptation for Category-level Object Pose Estimation," in *CVPR*, 2022, pp. 14871-14880.
- [68] R. Rasti, A. Biglari, M. Rezapourian, Z. Yang, and S. Farsiu, "RetiFluidNet: A Self-Adaptive and Multi-Attention Deep Convolutional Network for Retinal OCT Fluid Segmentation," *IEEE TMI*, vol. 42, no. 5, pp. 1413-1423, 2023.
- [69] C. Yang, H. Zhou, Z. An, X. Jiang, Y. Xu, and Q. Zhang, "Cross-image relational knowledge distillation for semantic segmentation," in *CVPR*, 2022, pp. 12319-12328.
- [70] G. J. Brostow, J. Shotton, J. Fauqueur, and R. Cipolla, "Segmentation and Recognition Using Structure from Motion Point Clouds," in *ECCV*, 2008, pp. 44-57.
- [71] M. Everingham, L. Van Gool, C. K. I. Williams, J. Winn, and A. Zisserman, "The Pascal Visual Object Classes (VOC) Challenge," *IJCV*, vol. 88, no. 2, pp. 303-338, 2010.